Blue phosphorene/$MoSi_2N_4$ van der Waals type-II heterostructure: Highly efficient bifunctional materials for photocatalytics and photovoltaics

Xiaohua Li(李晓华)[1], Baoji Wang(王宝基)[1,†], and Sanhuang Ke(柯三黄)[2]

[1] *School of Physics and Electronic Information Engineering, Henan Polytechnic University, Jiaozuo* 454000, *China*
[2] *MOE Key Laboratory of Microstructured Materials, School of Physics Science and Engineering, Tongji University, Shanghai* 200092, *China*

(Received 19 April 2022; revised manuscript received 7 August 2022; accepted manuscript online 23 September 2022)

Converting solar energy into electric power or hydrogen fuel is a promising means to obtain renewable green energy. Here, we design a two-dimensional blue phosphorene (BlueP)/$MoSi_2N_4$ van der Waals heterostructure (vdWH) and investigate its potential application in photocatalysis and photovoltaics using first-principles calculations. We find that the BlueP/$MoSi_2N_4$ vdWH possesses type-II band structure with a large build-in electric field, thus endowing it with a potential ability to separate photogenerated electron–hole pairs. The calculated band-edge positions show that the heterostructure is a very promising water-splitting photocatalyst. Its solar-to-hydrogen efficiency (η_{STH}) can reach up to 15.8%, which is quite promising for commercial applications. Furthermore, the BlueP/$MoSi_2N_4$ vdWH shows remarkably light absorption capacity and distinguished maximum power conversion efficiency (η_{PCE}) up to 10.61%. Remarkably, its η_{PCE} can be further enhanced by the external strain: the η_{PCE} of 21.20% can be obtained under a 4% tensile strain. Finally, we determine that adjusting the number of the BlueP sublayer is another effective method to modulate the band gaps and band alignments of the heterostructures. These theoretical findings indicate that BlueP/$MoSi_2N_4$ vdWH is a promising candidate for photocatalyst and photovoltaic device.

Keywords: *ab initio* study, heterostructure, photovoltaic cell, photocatalytic water splitting

PACS: 71.15.Mb, 71.20.–b, 71.20.Nr, 74.78.Fk **DOI:** 10.1088/1674-1056/ac9469

1. Introduction

Semiconductor photocatalysts have received much attention in recent years due to their great potentials for the development of clean energy technologies, as well as for environmental protection and remediation.[1–3] Specifically, two-dimensional (2D) materials are considered excellent candidates for solar cell and water-splitting photocatalyst because of their high specific surface areas and short migration path to the reaction surface for photoexcited electron–hole pairs.[4,5] Currently, a series of 2D materials such as transition metal carbides or nitrides,[6–9] transition-metal dichalcogenides (TMDs)[10,11] have been found to have great potential for photovoltaic and/or water-splitting applications. However, it is found that a pure semiconductor often cannot meet the requirements of practical applications. For example, the photogenerated carriers in such materials are not well separated spatially, which can lead to a fast electron–hole recombination and thus reduce the solar energy conversion. Fortunately, it is evident that establishing the 2D van der Waals heterostructure (vdWH) with the type-II band structure is a fascinating approach to conquer this challenge, where photoexcited electrons and holes are distributed separately in the two materials, thus prolonging carrier lifetime.[12,13] Typically, there are two major strategies regarding the construction of the 2D vdWHs: the top–down approach and bottom–up approach.[14] It is heartening to note that so far large amounts of 2D vdWHs are successfully constructed experimentally,[15,16] which makes their practical application possible in the future.

Recently, 2D layered phosphorus, which is a new member of the family of 2D materials, have gathered a great deal of attention due to their fascinating properties. Note that the carrier mobility of black phosphorene (BlackP) is 1000 $cm^2 \cdot V^{-1} \cdot s^{-1}$ at room temperature[17] which is considerably higher than that of a value 200 $cm^2 \cdot V^{-1} \cdot s^{-1}$ obtained by 2D layered TMDs. As an allotrope of BlackP, blue phosphorene (BlueP) has been successfully synthesized through molecular beam epitaxial growth on a Au (111) substrate by using the BlackP as a precursor.[18] Theoretical calculations indicate that the BlueP has a wider indirect gap and a higher hole mobility (1700 $cm^2 \cdot V^{-1} \cdot s^{-1}$) than that of BlackP.[19] Appropriate band edge alignments make it suitable for water splitting although it may suffer from low efficiency in separating photogenerated carriers.[13] And its photocatalytic properties can be modified by applying external strains or modulating layer numbers.[20] These properties make it a potential material for field effect transistors and other 2D electronic devices. Of course, we also note that both BlackP and BlueP have weak structural stability at ambient conditions in the presence of water and oxygen molecules.[21] The multilayer BlackP or BlueP is predicted to have better stability than its single layer due to the en-

†Corresponding author. E-mail: wbj@hpu.edu.cn

© 2023 Chinese Physical Society and IOP Publishing Ltd

hanced interlayer coupling and screening.[20,22] In this sense, constructing 2D BlueP-based vdWH can be considered to protect it from ambient degradation. So far, a large number of BlueP-based heterostructures have been studied. Our upfront works showed that BlueP/BSe and BlueP/$Mg(OH)_2$ vdWHs possess significant potency for water splitting reactions.[12,13] BlueP/Sc_2CX_2 (X = O, F) vdWHs have great potential in the field of photocatalysis and photovoltaics.[23] The work of Gao *et al*. showed that BlueP/g-GeC is a promising candidate for photocatalytic water splitting.[24] In short, BlueP is an excellent material to establish 2D vdWH with the high-efficiency photovoltaic and photocatalytic properties.

Recently, a new 2D layered material, $MoSi_2N_4$, has been successfully synthesized using the chemical vapor deposition (CVD) method.[6] Experimental results indicate that it has semiconducting characteristic (bandgap $\sim$ 1.94 eV) with good mechanical strength and air-stability. Motivated by the exciting properties of $MoSi_2N_4$, many efforts have been dedicated to revealing its novel properties and potential applications.[7,8,25] Specifically, $MoSi_2N_4$ monolayer owns high electron and hole mobilities, strong visible light absorption and suitable band edge positions for photocatalytic water splitting.[7,25] Similarly, the exotic properties of $MoSi_2N_4$ monolayer can be further tuned by combining with other 2D materials. To date, various $MoSi_2N_4$-based vdWHs have been investigated because they possess multitudinous new phenomena and unique properties.[26] For instance, Zeng *et al.* demonstrated that $MoSi_2N_4$ can be coupled with C_2N to form a typical type-II heterostructure with thermodynamic stability.[26] And this heterostructure is found to be a very promising photocatalyst for hydrogen production. Based on the aforementioned data, we reasonably speculate that the BlueP/$MoSi_2N_4$ vdWH may be a promising bifunctional materials and holds great potential to be synthesized in experiments.

In this work, we focus on the study of BlueP/$MoSi_2N_4$ vdWH as potential photocatalytic or photovoltaic materials. Its geometric structure, electronic structure, optical properties, and band edge, etc. are explored by performing first-principles calculations. The results show that BlueP/$MoSi_2N_4$ vdWH is a semiconductor with type-II band structure, which is conducive to the efficient separation of the photoexcited electron-hole pairs. Stronger optical absorption in the visible-UV light region is found compared with its components, along with the high solar-to-hydrogen (STH) and power conversion (PC) efficiencies, predicting its substantial potential in the field of solar energy utilization.

2. Methods

The density-functional theory (DFT) calculations are carried out by employing the Vienna *ab initio* simulation package (VASP)[27] with the projected augmented wave (PAW) method.[28] The DFT-D2 level[29] is adopted for the long-range vdW interaction. During structural optimization, the Perdew–Burke–Ernzerhof (PBE) functional and generalized gradient approximation (GGA) are used to calculate the electron exchange and correlation.[28] Dipole correction is employed to cancel the errors of electrostatic potential.[30,31] The cut-off energy is set to 500 eV. The thickness of the vacuum layer is set to 40 Å. The convergence criteria for the forces and energy are set to 0.01 eV/Å and 10^{-5} eV, respectively. The Heyd–Scuseria–Ernzerhof hybrid functional (HSE06)[32,33] is applied to obtain the precise electronic structures and optical properties. The $21 \times 21 \times 1$ and $9 \times 9 \times 1$ k-point meshes are used for PBE and HSE06 calculations, respectively. And in the HSE06 method, we adopt the mixing parameter of 0.125 and the screen factor of 0.20 $Å^{-1}$ to obtain a band gap close to the experimental value.

3. Results and discussion

The crystal structures of BlueP and $MoSi_2N_4$ monolayers are displayed in Figs. 1(a) and 1(c), respectively. The optimized lattice parameters of BlueP and $MoSi_2N_4$ monolayers are 3.27 Å and 2.91 Å, respectively, which in accordance with the previous predicted values.[6,19] The band structures of BlueP and $MoSi_2N_4$ monolayers are given in Figs. 1(b) and 1(d), respectively. Obviously, both BlueP and $MoSi_2N_4$ monolayers are indirect band gap semiconductors. For BlueP monolayer, its conduction band minimum (CBM) locates between the Γ and M points while the valence band maximum (VBM) locates between the K and Γ points. Its band gap is 2.35 eV using modified HSE06, which is closed to the previously reported data.[18,23] For the $MoSi_2N_4$ monolayer, its VBM and CBM are located at the Γ and the K point, respectively. The calculated band gap (2.06 eV) matches with experimental band gap of 1.94 eV.[6] We further note that polarization and spin–orbit coupling (SOC) effect have very small effects on the band dispersion for both the BlueP and $MoSi_2N_4$ monolayers (see Fig. A1). So we will neglect those effects in the following sections.

We now investigate geometric structures of the BlueP/$MoSi_2N_4$ vdWHs. A $\sqrt{3} \times \sqrt{3}$ BlueP monolayer and a $2 \times 2 \times 1$ $MoSi_2N_4$ monolayer are selected to build a nanocomposite with lattice constant of 5.79 Å. The lattice mismatch of such vdWH is small of 2.69%, which is accessible in experimental synthesis.[25,34] To search for the most stable pattern, four typical patterns are considered, namely, α-, β-, γ-, and δ-stacking. The structure of the BlueP/$MoSi_2N_4$ vdWH with α-stacking is presented in Fig. 2(a). Other patterns are shown in detail in Fig. A2 (see Appendix A). To compare the relative stabilities of the three stacking configurations, we calculate their interface binding energies,

$E_b = (E_H - E_P - E_M)/S$, where E_H, E_P, and E_M represent total energies of the BlueP/$MoSi_2N_4$ vdWH, BlueP and $MoSi_2N_4$ monolayers, respectively, and S is the surface area of the 2D supercell.[12,13] The lowest E_b of -423.97 meV·Å^{-2} is calculated in α-stacking associated with the nearest d of 3.438 Å. Meanwhile, we note that all the considered vdWHs possess very close negative E_b values, which means that they possess similar stabilities and are all stable. And we find that the stacking configurations have a minimal effect on the physical properties of the heterostructures (see Fig. A2(d)). Therefore, in the subsequent calculations, only BlueP/$MoSi_2N_4$ vdWH with α-stacking is discussed.

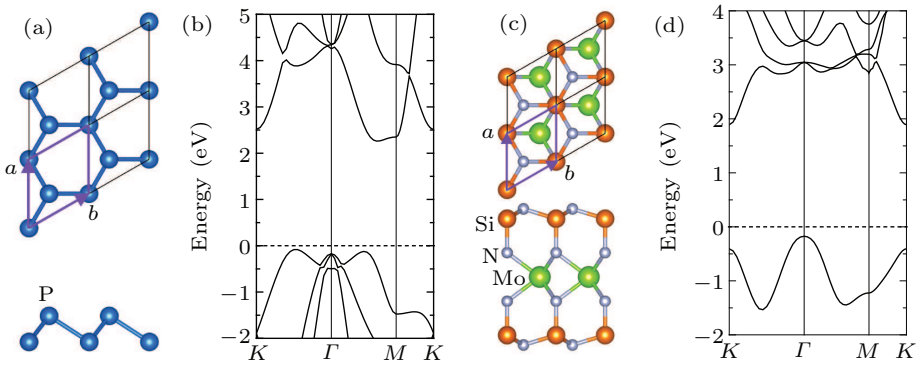


Fig. 1. Top and side views of the (a) BlueP and (c) $MoSi_2N_4$ monolayers. The violet rhombus indicates the primitive unit cell. The band structures given by the modified HSE06 for the (b) BlueP and (d) $MoSi_2N_4$ monolayers.

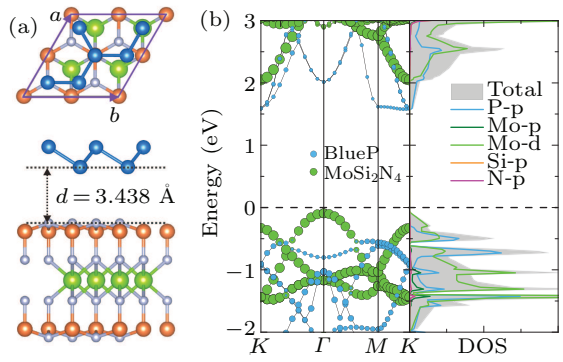


Fig. 2. (a) Top view (upper panel) and side view (down panel) of the BlueP/$MoSi_2N_4$ vdWH with α-stacking. The supercell boundary is denoted by violet rhombus. The optimized interlayer distance d is indicated. (b) The projected band structures of BlueP/$MoSi_2N_4$ vdWH using modified HSE06 calculation, in which the different colored spheres indicate the contributions from the different components. The corresponding total and partial density of states of the heterostructure are given in their right panels.

The projected band structure of the α-stacking BlueP/$MoSi_2N_4$ vdWH calculated by the amended HSE06 is illustrated in Fig. 2(b). Clearly, the VBM and CBM of the BlueP/$MoSi_2N_4$ vdWH locate at Γ point and K point, respectively, resulting in the feature of the indirect band gap. The calculated HSE06 band gap is predicted to be 1.67 eV, which satisfies the demands of water splitting ($\geq$ 1.23 eV) and fulfills the needs for efficient sunlight utilization (1.55 eV–3 eV).[35] Furthermore, the CBM is mainly contributed by the BlueP monolayer, while the VBM is dominated by the $MoSi_2N_4$ sublayer, which can be further confirmed from the partial density of states (PDOS) as shown in Fig. 2(b) (right panel). It can be found that the CBM mainly stems from the p states of P atoms, while the VBM state is mainly dominated by the d states of the Mo atoms. Hence, this vdWH has a type-II band alignment, which will spontaneously separate photogenerated electrons and holes, so as to achieve high efficiency solar energy conversion.

The interlayer interaction in the BlueP/$MoSi_2N_4$ vdWH will induce the charge transfer between two individuals, which can be analyzed by the charge density difference ($\Delta\rho(z)$) along the z direction. $\Delta\rho(z)$ can be determined by

$$\Delta\rho(z) = \rho_H(z) - \rho_B(z) - \rho_M(z), \tag{1}$$

where $\rho_H(z)$, $\rho_B(z)$, and $\rho_M(z)$ represent the charge densities of the BlueP/$MoSi_2N_4$ vdWH, the pristine BlueP and the $MoSi_2N_4$ monolayers, respectively. As shown in Fig. 3(a), some charges are transferred from the $MoSi_2N_4$ sheet to the BlueP layer. The amount of transferred electrons up to z point is determined by

$$\Delta Q(z) = \int_{-\infty}^{z} \Delta\rho(z)\,\mathrm{d}z. \tag{2}$$

The right y-axis of Fig. 3(a) unveils that about 0.61 electrons per unit cell is transferred from the $MoSi_2N_4$ layer to the BlueP sheet, which is calculated by the value of $\Delta Q(z)$ at the BlueP/$MoSi_2N_4$ interface.[36] The charge transfer induces an intrinsic built-in electric field (E_{in}) with its direction pointing from $MoSi_2N_4$ layer to BlueP layer, which can extend the recombination lifetime of the electron–hole pair. Moreover, the interface dipole moment $\mu(z)$ is also calculated by[37]

$$\mu(z) = \int z\Delta\rho(z)\,\mathrm{d}z. \tag{3}$$

Obviously, an inward pointing dipole is formed in the interface (see Fig. 3(b)).[37] That is to say, it points in the opposite direction of E_{in}, which will further suppress the recombination of photogenerated electrons and holes and prolong their life-span.

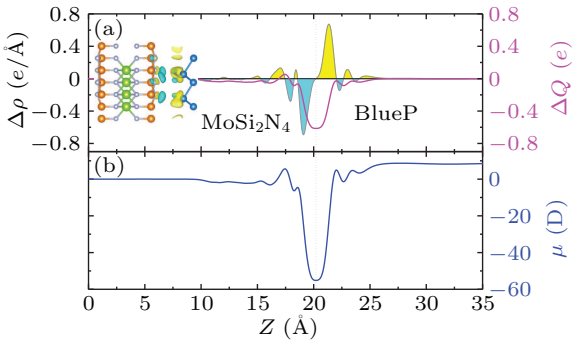


Fig. 3. (a) Plane-averaged charge density difference $\Delta\rho$ (gray line), the amount of transferred charge ΔQ (magenta line) and (b) interfacial dipole moment μ (blue line) along the normal direction of the heterostructure. The inset in (a) is the 3D isosurface of the charge density difference. The yellow and cyan areas represent electrons accumulation and depletion, respectively. The vertical dashed line denotes the BlueP/$MoSi_2N_4$ vdWH interface.

As mentioned above, the BlueP/$MoSi_2N_4$ vdWH has great potential as visible light photocatalyst. In order to evaluate its feasibility for water splitting, we align the band edge positions of heterostructure to the vacuum levels. As shown in Fig. 4(a), the band edges of the BlueP/$MoSi_2N_4$ vdWH can perfectly straddle the water redox potential at pH = 0, that is, the BlueP/$MoSi_2N_4$ vdWH can effectively promote the water splitting reaction due to the positive oxidation potential of VBM and the negative reduction potential of CBM. Besides, as we all know, the conduction band offset (CBO, ΔE_c) and valence band offset (VBO, ΔE_v) are crucial factors that affect the photocatalytic performance of the BlueP/$MoSi_2N_4$ vdWH. Here, the calculated ΔE_c and ΔE_v are around 0.82 eV and 0.29 eV, respectively.

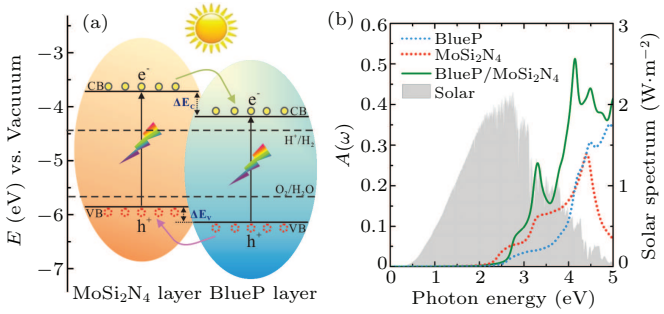


Fig. 4. (a) The band edge positions of the BlueP/$MoSi_2N_4$ vdWH are calculated within the HSE06 level. For comparison, the redox potentials of water splitting at pH = 0 are shown. (b) The optical absorption spectra $A(\omega)$ of BlueP, $MoSi_2N_4$ monolayers and BlueP/$MoSi_2N_4$ vdWH are also calculated based on HSE06 functional.

Moreover, we evaluate the STH efficiency (η_{STH}) of photocatalytic water splitting for BlueP/$MoSi_2N_4$ heterostructure as follows:[38]

$$\eta_{STH} = \frac{1.23\int_{E}^{\infty}\frac{P(h\omega)}{h\omega}\mathrm{d}(h\omega)}{\int_{0}^{\infty}P(h\omega)\mathrm{d}(h\omega)}, \quad (4)$$

where $P(h\omega)$ is the AM 1.5 solar energy flux at the photon energy of $h\omega$, E is the energy of photons that can actually be used for water splitting.[38–40] As a result, the η_{STH} of the BlueP/$MoSi_2N_4$ vdWH achieves 15.8%, which is economically viable as water-splitting photocatalyst.[38]

Besides, strong light absorption is also an important factor for solar applications. The absorption spectra of the BlueP/$MoSi_2N_4$ vdWH and the corresponding isolated layers are calculated and displayed in Fig. 4(b). The computational details have been fully described in our previous works.[12,13] Fascinatingly, the designed heterostructure shows more pronounced optical absorption in both visible and UV light region compared with the constituent monolayers, which suggests that the BlueP/$MoSi_2N_4$ vdWH has great potential as an efficient solar light absorber material.

We further estimate the maximum power conversion efficiencies (η_{PCE}) of the BlueP/$MoSi_2N_4$ heterostructure as photovoltaic solar cells by using the Scharber's method,[41] which is defined as follows:

$$\eta_{PCE} = \frac{0.65(E_g^d - \Delta E_c - 0.3)\int_{E_g^d}^{\infty}\frac{J(\hbar\omega)}{\hbar\omega}\mathrm{d}(\hbar\omega)}{\int_{0}^{\infty}P(\hbar\omega)\mathrm{d}(\hbar\omega)}, \quad (5)$$

where E_g^d and ΔE_c are the donor band gap and conduction band offset, respectively. $J(\hbar\omega)$ represents the AM 1.5 solar energy flux at the value of $\hbar\omega$ for photon energy. The calculated η_{PCE} value is about 10.61%, as marked in Fig. 5. And its η_{PCE} can be further enhanced by strain engineering (see later discussion). The results indicate that the BlueP/$MoSi_2N_4$ vdWH can also be a promising photovoltaic material.

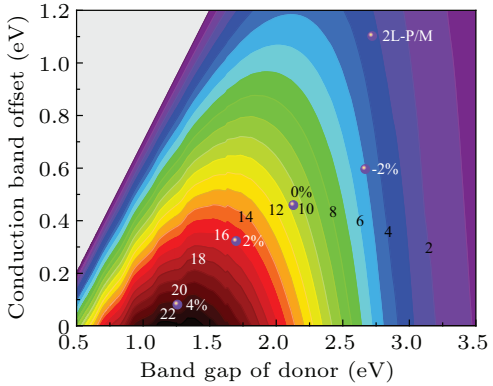


Fig. 5. Power conversion efficiency contour. The spheres on the contour represent the efficiency limits of the BlueP/$MoSi_2N_4$ heterostructures under the different strains. The η_{PCE} value of the 2L-P/M heterostructure is also labeled.

Next, we will explore the effect of strain on the photocatalytic and photovoltaic properties of the BlueP/$MoSi_2N_4$ vdWH. Here, the applied in-layer biaxial strain ε is defined by $\varepsilon = (a - a_0)/a_0 \times 100\%$, where a and a_0 represent the lattice constants for the strained and unstrained structures, respectively. Meanwhile, the strain energy per atom is also calculated as follows $E_s = (E_{strained} - E_{unstrained})/n$, where n is the number of atoms in the unit cell. As shown in Fig. 6(a), when the compressive strain decreases from −8% to −4%,

the band gap increases gradually and reaches its maximum value (~ 2.22 eV) at $\varepsilon = -4\%$. When the strain varies from -4% to $+8\%$, its band gap decreases monotonically. From Fig. 6(a) (right y-axis), we also find that the strain energy curve is smooth as a quadratic function under the biaxial strain, indicating that all the strains considered are within the elastic limit.

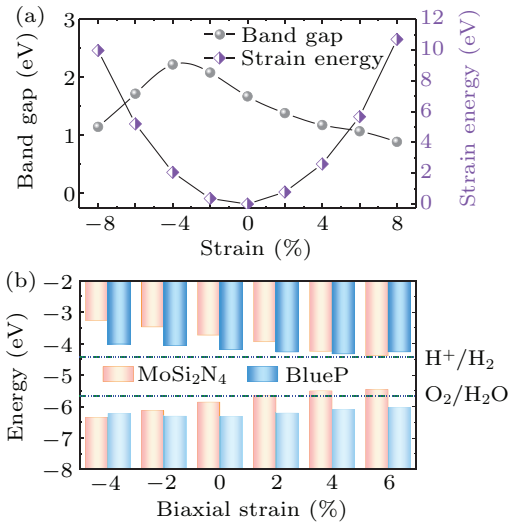


Fig. 6. (a) Calculated band gap and strain energy, and (b) the band-edge positions of the BlueP/$MoSi_2N_4$ vdWH under different biaxial strains by the HSE06 functional. The standard redox potentials of water splitting (at pH = 0) are denoted by the dashed line.

The band edge positions of the BlueP/$MoSi_2N_4$ vdWH under different biaxial strain are plotted in Fig. 6(b). Obviously, under compression-to-tension strains, the VBM and CBM of BlueP layer remain nearly constant, while the VBM (CBM) of $MoSi_2N_4$ layer moves up (down). As a result, the greater compressive or tensile strains induce a transition from type-II to type-I band alignment, which is detrimental to photocatalysis.[42] However, the type-II band alignment properties are maintained under a moderate strain ($-2\% \leq \varepsilon \leq +4\%$). In particular, when $\varepsilon = -2\%$, its CBM and VBM overpotentials are all closed to 0.4 eV, which is adequate for H_2/O_2 production from water. Besides, we note that the tensile strain effectively reduces the E_g^d and ΔE_c, thus significantly improving the η_{PCE}. A η_{PCE} as high as $\sim 21.20\%$ can be achieved under the 4% tensile strain, as marked in Fig. 5. Hence, the tensile strain is an effective way to enhance the η_{PCE} of the BlueP/$MoSi_2N_4$ vdWH.

Finally, we will focus on the effect of multilayer BlueP on the electronic properties of the $MoSi_2N_4$-based vdWHs. Here, we consider two cases: bilayer BlueP/$MoSi_2N_4$ (2L-P/M) and trilayer BlueP/$MoSi_2N_4$ (3L-P/M) heteromultilayers, as illustrated in Figs. 7(a) and 7(c), respectively. The multilayer BlueP adopts the stable AA-stacking configurations.[20] The band structures are shown in Figs. 7(b) and 7(d), respectively. As can be seen, the heteromultilayers are all indirect semiconductors and the band gaps decrease with the increase of the thickness owing to the quantum confinement effect. The 2L-P/M heterostructure forms a type-II alignment, similar to heterobilayers, whereas the 3L-P/M heterostructure forms a type-I alignment, which implies that altering the number of constituent layers can lead to the transition from type-II to I. In the meantime, we find that the 2L-P/M heterostructure is also a promising water splitting material with a practical η_{STH} value ($\sim 15.6\%$). Unfortunately, the multilayer BlueP dramatically increases the ΔE_c, thus significantly decreasing the η_{PCE}. The calculated η_{PCE} value of 2L-P/M heterostructure is only 3.2%, as marked in Fig. 5. For 3L-P/M heterostructure, type-I band alignment and inappropriate band edge positions make it unsuitable for water splitting or photovoltaic solar cells.

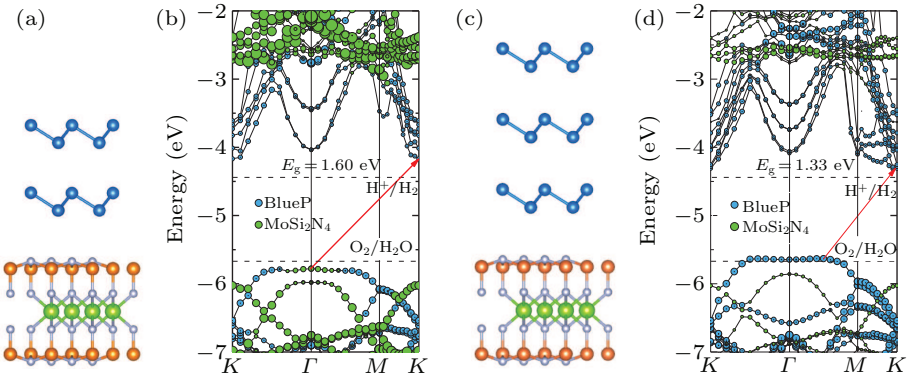


Fig. 7. Side views of (a) 2L-P/M and (c) 3L-P/M heterostructures. Projected band structures with modified HSE06 functional of (b) 2L-P/M and (d) 3L-P/M heterostructures, referring to the vacuum level. The redox potentials (dashed line) of water splitting are shown for comparison.

4. Conclusion

In this paper, we have investigated the electronic, optical, photocatalytic and photovoltaic properties of the BlueP/$MoSi_2N_4$ vdWH based on the first principles calculations. Our findings indicate that BlueP/$MoSi_2N_4$ vdWH is an indirect-band-gap semiconducting material with type-II band alignment. With the combination of suitable band gaps, proper bandedge positions, effective separation of carriers and high STH efficiency, the BlueP/$MoSi_2N_4$ vdWH shows great possibility to be used as photocatalysts for water splitting. Compared with its composing BlueP and $MoSi_2N_4$ monolayers,

the heterostructure exhibits more efficient optical absorption. Also, the BlueP/$MoSi_2N_4$ vdWH is found to have potential for application in photovoltaic cell. Further investigations reveal that its photocatalytic and photovoltaic properties can be significantly modulated by external uniform strains. Especially, a 4% strain will increase its η_{PCE} by about 99.9%. The layer-dependent behavior of the BlueP/$MoSi_2N_4$ vdWH is also studied. All these data strongly suggest that BlueP/$MoSi_2N_4$ vdWH is a very promising photocatalytic and photovoltaic material.

Appendix A

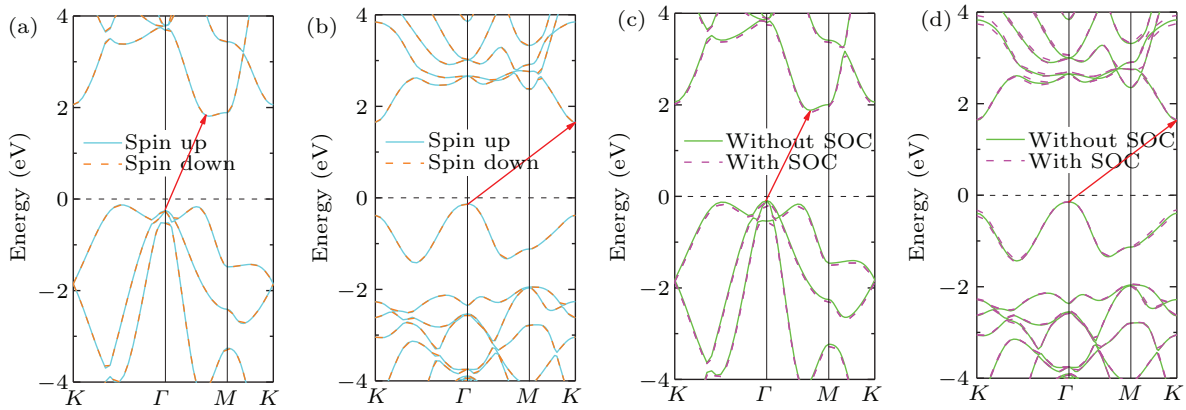


Fig. A1. The calculated band structures of (a) BlueP and (b) $MoSi_2N_4$ monolayers by considering spin polarization. Band structures of (c) BlueP and (d) $MoSi_2N_4$ monolayers with and without spin–orbit coupling (SOC) effect. The results are from the vdW-DFT/PBE calculations.

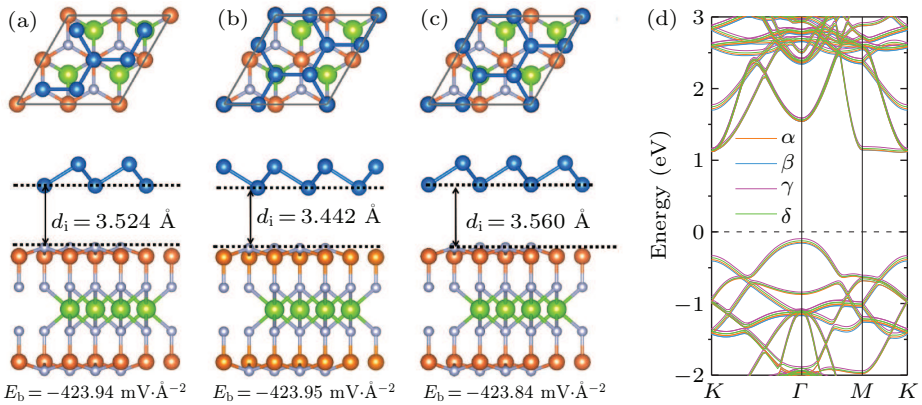


Fig. A2. Top (upper panel) and side (lower panel) views of the BlueP/$MoSi_2N_4$ heterostructures with different stacking sequences: (a) β-stacking, (b) γ-stacking, and (c) δ-stacking. The corresponding interlayer distances (d_i) and binding energies (E_b) are also labeled. (d) Band structures of the BlueP/$MoSi_2N_4$ heterostructures with α-, β-, γ- and δ-stacking given by the PBE functional.

Acknowledgements

Project supported by the National Natural Science Foundation of China (Grant No. 11374226), the Fundamental Research Funds for the Universities of Henan Province of China (Grant No. NSFRF200331), the Foundation of Henan Educational Committee (Grant No. 20A140013), as well as by the High-performance Grid Computing Platform of Henan Polytechnic University.

References

[1] Hou H and Zhang X 2020 *Chem. Eng. J.* **395** 125030

[2] Xie Z, Peng Y, Yu L, Xing C, Qiu M, Hu J and Zhang H 2020 *Solar. RRL* **4** 1900400

[3] Xie Z, Duo Y, Lin Z, Fan T, Xing C, Yu L, Wang R, Qiu M, Zhang Y, Zhao Y, Yan X and Zhang H 2020 *Adv. Sci.* **7** 1902236

[4] Singh A K, Mathew K, Zhuang H L and Hennig R G 2015 *J. Phys. Chem. Lett.* **6** 1087

[5] Wang L, Huang L, Tan W, Feng X, Chen L, Huang X and Ang K 2018 *Small Methods* **2** 1700294

[6] Hong Y L, Liu Z, Wang L, Zhou T, Ma W, Xu C, Feng S, Chen L, Chen M L, Sun D M, Chen X Q, Cheng H and Ren W 2020 *Science* **369** 670

[7] Mortazavi B, Javvaji B, Shojaei F, Rabczuk T, Shapeev A V and Zhuang X 2021 *Nano Energy* **82** 105716

[8] Yao H, Zhang C, Wang Q, Li J, Yu Y, Xu F, Wang B and Wei Y 2021 *Nanomaterials* **11** 559

[9] Gao L, Chao Li, Huang W, Mei S, Lin H, Ou Q, Zhang Y, Guo J, Zhang F, Xu S and Zhang H 2020 *Chem. Mater.* **32** 1703

[10] Zhuang H L and Hennig R G 2013 *J. Phys. Chem. C* **117** 20440

[11] Zhuang H L, Johannes M D, Blonsky M N and Hennig R G 2014 *Appl. Phys. Lett.* **104** 022116

[12] Wang B J, Li X H, Cai X L, Yu W Y, Zhang L W, Zhao R and Ke S H 2018 *J. Phys. Chem. C* **122** 7075

[13] Wang B J, Li X H, Zhao R Q, Cai X L, Yu W Y, Li W B, Liu Z S, Zhang L W and Ke S H 2018 *J. Mater. Chem. A* **6** 8923

[14] Liu L X and Zha T Y 2021 *InfoMat.* **3** 3

[15] Li J, Yang X D, Liu Y, Huang B L, Wu R X, Zhang Z W, Zhao B, Ma H F, Dang W Q, Wei Z, Wang K, Lin Z Y, Yan X X, Sun M Z, Li B, Pan X Q, Luo J, Zhang G Y, Liu Y, Huang Y, Duan X D and Duan X F 2020 *Nature* **579** 368

[16] Ahsan M A, He T W, Noveron J C, ReuterK, Puente-Santiago A R and Luque R 2022 *Chem. Soc. Rev.* **51** 812

[17] Li L, Yu Y, Ye G J, Ge Q, Ou X, Wu H, Feng D, Chen X H and Zhang Y 2014 *Nat. Nanotechnol.* **9** 372

[18] Zhang J L, Zhao S, Han C, Wang Z, Zhong S, Sun S, Guo R, Zhou X, Gu C D, Yuan K D, Li Z and Chen W 2016 *Nano Lett.* **16** 4903

[19] Xiao J, Long M Q, Zhang X J, Ouyang J, Xu H and Gao Y L 2015 *Sci. Rep.* **5** 09961

[20] Wang J J, Li S C, Yun F Y, Zhang X and Li Q X 2020 *Int. J. Quantum Chem.* **120** e26230

[21] Wang G X, Slough W J, Pandey R and Karna S P 2016 *2D Mater.* **3** 025011

[22] Cai Y Q, Zhang G and Zhang Y W 2014 *Sci. Rep.* **4** 6677

[23] Li X H, Wang B J, Wang G D and Ke S H 2020 *Sustain. Energ. Fuels* **4** 5277

[24] Gao X, Na Y S, Ma Y Y, Wu S Y and Zhou Z X 2019 *Appl. Phys. Lett.* **114** 093902

[25] Bafekry A, Faraji M, Hoat D M, Fadlallah M M, Shahrokhi M, Shojaei F, Gogova D and Ghergherehchi M 2021 *J. Phys. D: Appl. Phys.* **54** 155303

[26] Zeng J, Xu L, Yang Y W, Luo X, Li H J, Xiong S X and Wang L L 2021 *Phys. Chem. Chem. Phys.* **23** 8318

[27] Kresse G and Hafner J 1993 *Phys. Rev. B* **47** 558

[28] Perdew J P, Burke K and Ernzerhof M 1996 *Phys. Rev. Lett.* **77** 3865

[29] Grimme S 2006 *J. Comput. Chem.* **27** 1787

[30] Li J, Liu W Q, Zhou W H, Yang J L, Qu H Z, Hu Y and Zhang S L 2022 *Phys. Rev. Appl.* **17** 054009

[31] Li J, Zhou W H, Xu L L, Yang J L, Qu H Z, Guo T T, Xu B, Zhang S L and Zeng H B 2022 *Mater. Today Phys.* **26** 100749

[32] Heyd J, Scuseria G E and Ernzerhof M 2003 *J. Chem. Phys.* **118** 8207

[33] Heyd J, Scuseria G E and Ernzerhof M 2006 *J. Chem. Phys.* **124** 219906

[34] Peng Q, Wang Z, Sa B, Wu B and Sun Z 2016 *Sci. Rep.* **6** 31994

[35] Yu Y, Zhou J and Sun Z 2020 *Adv. Funct. Mater.* **30** 2000570

[36] Cai Y Q, Zhang G and Zhang Y W 2015 *J. Phys. Chem. C* **119** 13929

[37] He C, Zhang J H, Zhang W X and Li T T 2019 *J. Phys. Chem. Lett.* **10** 3122

[38] Fu C F, Sun J Y, Luo Q Q, Li X X, Hu W and Yang J L 2018 *Nano Lett.* **18** 6312

[39] Lu B, Zheng X and Li Z 2020 *Nanoscale* **12** 6617

[40] Yang H, Ma Y, Zhang S, Jin H, Huang B and Dai Y 2019 *J. Mater. Chem. A* **7** 12060

[41] Scharber M C, Mühlbacher D, Koppe M, Denk P, Waldauf C, Heeger A J and Brabec C 2006 *Adv. Mater.* **18** 789

[42] Cheng Z, Wang F, Shifa T A, Jiang C, Liu Q and He J 2017 *Small* **13** 1702163